Optimized coupling conditions for discrete fracture matrix models

Martin J. Gander, Julian Hennicker, Roland Masson

1 Introduction

In [7, 8], we derived and studied an asymptotic model for Darcy flow in fractured porous media, when the fracture aperture δ is approaching zero. We showed that our new, general models coincide in special cases with common models from the literature, as e.g. [11, 2, 10, 1]. Our general modeling approach leads to coupling conditions, which are suitable for small fracture aperture and for a resolution of low frequencies k. It also permits several adaptations, one of which we explore here, namely new coupling conditions with extended range of validity, obtained by replacing the parameters in the asymptotic coupling conditions by new parameters, which we then optimize w.r.t. the error for a given range of frequency components $k \in [k_{\min}, k_{\max}]$ present in the numerical solution to be computed. Our results are based on the explicit formula from [8] for the error for the solution of the asymptotic model in Fourier space, which we adapt to generalized parameters. In order to obtain explicit formulas for the optimized parameters, we make some simplifying assumptions, and then solve the resulting optimization problem analytically using asymptotic techniques for small fracture apertures. Our approach could also be adapted to more general situations, and we could have chosen to use expansions for $\delta \to \delta_0$ or $k \to k_\infty$, with δ_0 or k_∞ a fixed constant, for example. In this sense, we want to outline conceptually a technique to improve the model accuracy for the model in [7], which can be adapted by the reader to the situation at hand. An ad hoc generalisation to fracture networks would be to apply the matrix-fracture coupling conditions, as derived in our manuscript, to each of the fracture segments and to

Martin J. Gander
Université de Genève, e-mail: martin.gander@unige.ch

Julian Hennicker
Université du Luxembourg, e-mail: julian.hennicker@uni.lu

Roland Masson
Université Côte d'Azur, CNRS, e-mail: roland.masson@unice.fr

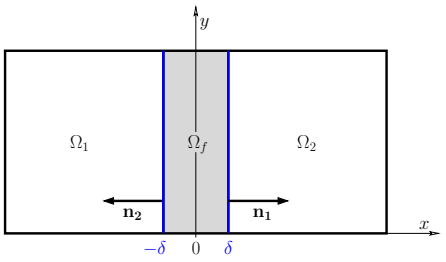

Fig. 1 Geometry of the domain under consideration.

impose pressure continuity and flux conservation at the fracture intersections (see e.g. [9], or [3] for an alternative formulation in the case of highly contrasted fracture permeabilities). A rigorous treatment of cross points in domain decomposition is a topic of substantial interest for current research (cf. [6], and references therein), and its application to fracture intersections is a project for future work.

2 Model problem

In the domains illustrated in Fig. 1, we consider the system of PDEs

$$-\mathrm{div}\mathbf{q}_j + \frac{\mathbf{b}_j}{2}\cdot\nabla u_j + (\eta_j - \mathrm{div}\frac{\mathbf{b}_j}{2})u_j = h_j \quad \text{in} \quad \Omega_j,\ j = 1,2,f, \tag{1}$$

$$\mathbf{q}_j = (\mathbf{A}_j\nabla - \frac{\mathbf{b}_j}{2})u_j \quad \text{in} \quad \Omega_j,\ j = 1,2,f, \tag{2}$$

connected at $x = \pm\delta$ with the coupling conditions

$$u_j = u_f \quad \text{on} \quad \partial\Omega_j \cap \partial\Omega_f,\ j = 1,2, \tag{3}$$

$$\mathbf{q}_j\cdot\mathbf{n}_j = \mathbf{q}_f\cdot\mathbf{n}_j \quad \text{on} \quad \partial\Omega_j \cap \partial\Omega_f,\ j = 1,2. \tag{4}$$

The model coefficients are $\eta_j : \Omega_j \to \mathbb{R}_{\geq 0}$, $\mathbf{b}_j : \Omega_j \to \mathbb{R}^2$, such that $\eta_j - \mathrm{div}\mathbf{b}_j \geq 0$, and coercive matrices $\mathbf{A}_j : \Omega_j \to \mathbb{R}^{2\times 2}$. The model unknowns are $\mathbf{q}_j$ and u_j. For this problem, we can eliminate the fracture unknowns in Fourier space, as described in [8]: applying a Fourier transform in the direction tangential to the fracture, the fracture Fourier coefficients have to satisfy specific ODEs which can be solved using two of the four coupling conditions at the interfaces. Then, the fracture solution is substituted into the remaining two coupling conditions. The resulting equations at $x = \pm\delta$ for the coupling between the matrix domains, when the fracture has been eliminated, are

$$\hat{\mathbf{q}}_2 \cdot \mathbf{n}_2 + \hat{\mathbf{q}}_1 \cdot \mathbf{n}_1 = -a_{11}\sqrt{\frac{a_{22}}{a_{11}}k^2}\tanh\left(\delta\sqrt{\frac{a_{22}}{a_{11}}k^2}\right)(\hat{u}_1 + \hat{u}_2), \tag{5}$$

$$\hat{\mathbf{q}}_2 \cdot \mathbf{n}_2 - \hat{\mathbf{q}}_1 \cdot \mathbf{n}_1 = \frac{a_{11}\sqrt{\frac{a_{22}}{a_{11}}k^2}}{\tanh\left(\delta\sqrt{\frac{a_{22}}{a_{11}}k^2}\right)}(\hat{u}_2 - \hat{u}_1), \tag{6}$$

under the simplifying assumption that $h_f \equiv 0$, $\mathbf{b}_f = 0$, $\eta_f = 0$, and $\mathbf{A}_f$ being diagonal.

Asymptotic coupling for small δ. We recall first the asymptotic coupling conditions for small δ presented in [8]. For $\delta \to 0$, we can expand

$$\tanh\left(\delta\sqrt{\frac{a_{22}}{a_{11}}k^2}\right) = \delta\sqrt{\frac{a_{22}}{a_{11}}k^2} - \delta^3\frac{1}{3}\sqrt{\frac{a_{22}}{a_{11}}k^2}^3 + O(\delta^5). \tag{7}$$

Truncation after the next-to-leading-order term yields at $x = \pm\delta$ the reduced order coupling conditions

$$\hat{\mathbf{q}}_1^{\text{red}} \cdot \mathbf{n}_1 + \hat{\mathbf{q}}_2^{\text{red}} \cdot \mathbf{n}_2 = -\delta a_{22}k^2(\hat{u}_1^{\text{red}} + \hat{u}_2^{\text{red}}), \tag{8}$$

$$\hat{\mathbf{q}}_1^{\text{red}} \cdot \mathbf{n}_1 - \hat{\mathbf{q}}_2^{\text{red}} \cdot \mathbf{n}_1 = \frac{a_{11}}{\delta}(\hat{u}_2^{\text{red}} - \hat{u}_1^{\text{red}}). \tag{9}$$

3 Generalized coupling conditions and their optimization

The coupling conditions (8) and (9) are by construction most suitable for small values of δ, and also for small values of k, due to a symmetry between δ and k. In practical numerical computations, the solution sought has however a certain range of frequencies, $k \in [k_{\min}, k_{\max}]$, not only low ones. To treat such a wider range of frequencies, we use now a common technique from Optimized Schwarz methods in domain decomposition [4, 5], which consists in keeping the structure of the reduced order coupling conditions, and introducing new parameters as d.o.f. for a subsequent optimization. In our case, the coupling conditions are of Robin type, and we replace the occurring parameters in (8) and (9), δa_{22} and $\frac{a_{11}}{\delta}$, by newly introduced parameters p and q, which gives the optimizable reduced coupling conditions

$$\hat{\mathbf{q}}_1^{\text{red}} \cdot \mathbf{n}_1 + \hat{\mathbf{q}}_2^{\text{red}} \cdot \mathbf{n}_2 = -pk^2(\hat{u}_1^{\text{red}} + \hat{u}_2^{\text{red}}),$$
$$\hat{\mathbf{q}}_1^{\text{red}} \cdot \mathbf{n}_1 - \hat{\mathbf{q}}_2^{\text{red}} \cdot \mathbf{n}_1 = q(\hat{u}_2^{\text{red}} - \hat{u}_1^{\text{red}}).$$

In [8], the error at the interfaces of the δ-asymptotic reduced order solution in Fourier space was derived, see the result after eq. (7.5) therein. The errors for our generalized reduced order model can analogously be obtained, and we get for $j = 1, 2$

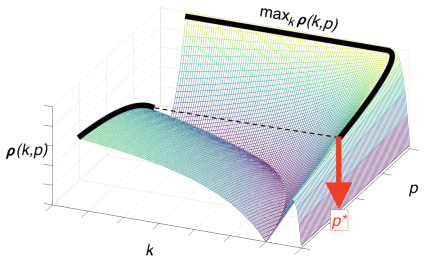

Fig. 2 Illustration of how to find a solution to (14) and (15).

$$\begin{aligned}\hat{e}_j &:= \hat{u}_j - \hat{u}_j^{\text{red}} \\ &= \rho(k,p)(\hat{u}_2 + \hat{u}_1) + (-1)^{j+1}\tau(k,q)(\hat{u}_2 - \hat{u}_1),\end{aligned} \tag{10}$$

where

$$\rho(k,p) = -\frac{1}{2}\frac{\sqrt{a_{11}a_{22}k^2}\tanh(\delta\sqrt{\frac{a_{22}}{a_{11}}k^2}) - pk^2}{\sqrt{k^2 + pk^2}}, \tag{11}$$

$$\tau(k,q) = \frac{1}{2}\frac{\frac{\sqrt{a_{11}a_{22}k^2}}{\tanh(\delta\sqrt{\frac{a_{22}}{a_{11}}k^2})} - q}{\sqrt{k^2 + q}}. \tag{12}$$

In order to minimize the error for a range of frequencies in a simulation, we need to solve

$$\min_{p,q}\max_{k\in(k_{\min},k_{\max})} |\hat{e}_j(k,p,q)|, \tag{13}$$

for small $\delta \ll k_{\max}^{-1}$. Since $(\hat{u}_2 + \hat{u}_1)$ and $(\hat{u}_2 - \hat{u}_1)$ are linearly independent, our objective functions to be minimized are $|\rho|$ and $|\tau|$. The following lemma will be applied without proof.

Lemma 1 *The solution* (k^*, p^*, q^*) *to*

$$\partial_k\rho(k^*,p^*) = 0 \tag{14}$$

$$|\rho(k_{\max},p^*)| = |\rho(k^*,p^*)| \tag{15}$$

$$|\tau(k_{\max},q^*)| = |\tau(k_{\min},q^*)| \tag{16}$$

solves the relevant min-max problem (13)*.*

We will first solve for the equation (16), and then for the independent problem (14) and (15), cf. Fig. 2. Since we are interested in the case of fracture apertures, which are not resolved by the mesh, i.e. $\delta \ll k_{\max}^{-1}$, we will solve the problem asymptotically in δ, for the leading and next–to–leading order terms of the expansions.

First, using the asymptotic expansion (7) in (12) yields

$$\tau(k,q) = \frac{1}{2}\frac{\frac{a_{11}}{\delta} + \frac{a_{22}\delta k^2}{3} - q}{|k| + q} + O(\delta^3). \tag{17}$$

Inserting this into (16) implies

$$\frac{\frac{a_{11}}{\delta} + \frac{a_{22}\delta k_{\min}^2}{3} - q^*}{|k_{\min}| + q^*} + \frac{\frac{a_{11}}{\delta} + \frac{a_{22}\delta k_{\max}^2}{3} - q^*}{|k_{\max}| + q^*} = O(\delta^3). \tag{18}$$

Hence,

$$\begin{aligned} q^* = {} & \frac{a_{11}}{2\delta} + \frac{a_{22}\delta k_{\max}^2 + k_{\min}^2}{12} - \frac{k_{\max} + k_{\min}}{4} \\ & + \Big[(\frac{a_{11}}{2\delta})^2 + \frac{a_{11}(k_{\min} + k_{\max})}{4\delta} + \Big(\frac{k_{\min} + k_{\max}}{4}\Big)^2 + \frac{a_{11}a_{22}(k_{\min}^2 + k_{\max}^2)}{12} \\ & + \frac{a_{22}\delta}{12}\Big(\frac{1}{2}(k_{\min} + k_{\max})^3 - (k_{\min}^3 + k_{\max}^3)\Big) + \Big(\frac{a_{22}\delta}{12}(k_{\min} + k_{\max})\Big)^2 \Big]^{\frac{1}{2}}. \end{aligned} \tag{19}$$

We can now derive an asymptotic formula for the optimized error in the jump of u across the fracture by substituting the optimized parameter q^* into τ, at $k = k_{max}$ or equivalently at $k = k_{\min}$, and obtain

$$\begin{aligned} & \min_q \max_{k\in(k_{\min},k_{\max})} |\tau(k,q)| \\ & \quad = |\tau(k_{\max},q^*)| = |\tau(k_{\min},q^*)| = \frac{a_{22}(k_{\max}^2 - k_{\min}^2)}{12a_{11}}\delta^2 + O(\delta^3). \end{aligned} \tag{20}$$

This result can further be compared to the corresponding error of the original model,

$$\max_{k\in(k_{\min},k_{\max})} |\tau(k,\frac{a_{11}}{d})| = \frac{a_{22}k_{\max}^2}{6a_{11}}\delta^2 + O(d^3). \tag{21}$$

We observe that the asymptotic constant in (20) is approximately half the value of the asymptotic constant in (21). For solving for (14) and (15), we can proceed analogously: first, we use the expansion (7) in (11), and obtain

$$\rho(k,p) = -\frac{1}{2}\frac{a_{22}\delta - \frac{a_{22}^2\delta^3k^2}{3a_{11}} - p}{(p + \frac{1}{|k|})} + O(\delta^4). \tag{22}$$

Substituting (22) into (14) and (15) implies

$$-\frac{-3a_{11}\,(a_{22}d - p^*) + 2a_{22}^2d^3k^{*2}\,(k^*p^* + 1) + a_{22}^2d^3k^{*2}}{3a_{11}\,(k^*p^* + 1)^2} = O(\delta^4), \tag{23}$$

$$\frac{a_{22}\delta - \frac{a_{22}^2\delta^3k^{*2}}{3a_{11}} - p^*}{(p^* + \frac{1}{|k^*|})} + \frac{a_{22}\delta - \frac{a_{22}^2\delta^3k_{\max}^2}{3a_{11}} - p^*}{(p^* + \frac{1}{|k_{\max}|})} = O(\delta^4). \tag{24}$$

Solving (23) and (24), we obtain the optimized parameters

$$k^* = \frac{k_{\max}}{2} + \mathcal{O}(\delta^4) \quad \text{and} \quad p^* = a_{22}\delta - \frac{a_{22}^2\delta^3 k_{\max}^2}{4a_{11}} + \mathcal{O}(\delta^4). \tag{25}$$

Finally, we obtain an asymptotic formula for the optimized error in the averaged traces of u at the interface, by substituting the optimized parameters into ρ,

$$\min_p \max_{k\in(k_{\min},k_{\max})} |\rho(k,p)| = |\rho(k_{\max},p^*)| = |\rho(k^*,q^*)| = \frac{a_{22}^2 k_{\max}^3}{24a_{11}}\delta^3 + \mathcal{O}(\delta^4). \tag{26}$$

We can again compare this to the error of the original model,

$$\max_{k\in(k_{\min},k_{\max})} |\rho(k,a_{22}\delta)| = \frac{a_{22}^2 k_{\max}^3}{6a_{11}}\delta^3 + \mathcal{O}(\delta^4), \tag{27}$$

and observe that the asymptotic constant in (26) is a fourth of the value of the asymptotic constant in (27).

4 Numerical results

We will now illustrate our results numerically and compare the theoretical error of the optimized problem with parameters p^* and q^*, for which we have the expressions (25) and (19), with the theoretical error of the asymptotic model (8), (9) from [7, 8], which employs the parameters

$$q^{\text{red}} = \frac{a_{11}}{\delta} \quad \text{and} \quad p^{\text{red}} = a_{22}\delta.$$

These parameters have been calculated analytically, for small fracture apertures. On the other hand, we can solve the problem (13) numerically for any given data, and thus obtain general optimized parameters, which will serve as reference parameters, and which we will denote by p^{opt} and q^{opt}. We will also show plots of the corresponding errors

$$\max_{k\in(k_{\min},k_{\max})} |\tau(k,q)| \quad \text{and} \quad \max_{k\in(k_{\min},k_{\max})} |\rho(k,p)|,$$

for $q \in \{q^{\text{opt}}, q^*, q^{\text{red}}\}$ and $p \in \{p^{\text{opt}}, p^*, p^{\text{red}}\}$. When interpreting the results, the reader is referred to (10). Please also note that the jump $\hat{u}_2 - \hat{u}_1$ is of order δ, as shown in [8]. We present three different cases: homogeneous isotropic fractures, fracture barriers, and fracture conduits. The fracture apertures are from 10^{-2} to 10^{-5} and the frequency range is set to $[k_{\min} = 0, k_{\max} = \pi]$, on an infinite domain.

Homogeneous isotropic fracture. This is a fracture with the same properties as the bulk domain, i.e. $a_{11} = a_{22} = 1$. The plots in Fig. 3 show the theoretical errors of

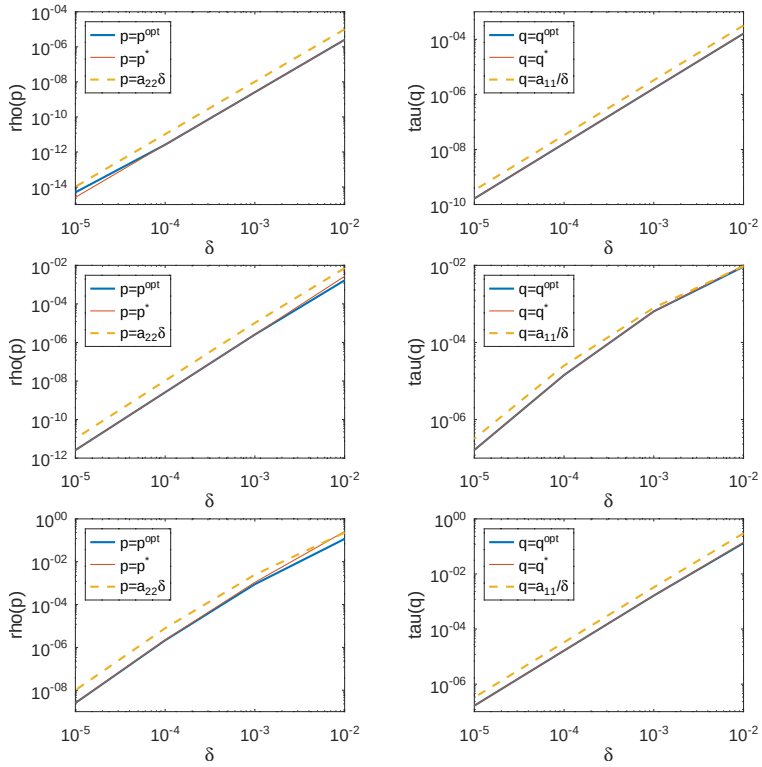

Fig. 3 Isotropic fracture, fracture barrier and fracture conduit (from top to bottom). Exact errors for the asymptotic, asymptotic optimized, and numerically optimized parameters.

the reduced order solutions, and their convergence to the reference solution, with $\delta \to 0$. We observe that the error of the asymptotic optimized model is in very good agreement with the error of the numerically optimized model for all δ. The slight difference in ρ for $\delta = 10^{-5}$ is due to round-off error, as we have reached machine precision. The error plots also reveal an advantage of the optimized models over the asymptotic model from [7]. The gain in accuracy can be analytically quantified by the ratios of asymptotic constants in (20) and (21) for τ, and in (26) and (27) for ρ.

Fracture barrier. Let us consider anisotropic diffusion coefficients in the fracture: a very low normal diffusion $a_{11} = 10^{-3}$ and a homogeneous tangential diffusion $a_{22} = 1$. Similar to the isotropic test case, we observe from the plots in Fig. 3 an advantage of the optimized models over the asymptotic model from [7], which can be quantified by looking at the asymptotic coefficients in (20) and (21) for τ, and in (26) and (27) for ρ. We observe that the error of the asymptotic optimized model is in very good agreement with the error of the numerically optimized model for all δ, except for $\delta = 10^{-2}$, where there is a small difference. This is due to the strong heterogeneity and anisotropy of the fracture diffusion coefficients, which have not been accounted for in the derivation of the optimized parameters.

Fracture conduit. Let us now consider a high tangential diffusion $a_{22} = 10^3$ and a homogeneous normal diffusion $a_{11} = 1$. The results shown in Fig. 3 are comparable to the results from the previous test case.

5 Conclusion

We presented a new way to generalize the coupling conditions from [7, 8] for discrete fracture matrix models to a wider range of frequencies arising in the numerical solution. To do so, we conserved the structure of the original coupling conditions obtained for small fracture apertures, but optimized the occurring parameters for a given range of numerical frequencies, with the error as the objective function. This led to the new optimized parameters given in (19) and (25), which minimize the error committed by the reduced order model. We also quantified the error by comparing the asymptotic coefficients in the equations (20) and (21) for the error in the pressure jump across the fracture, and in (26) and (27) for the error in the averaged pressure across the fracture. This comparison shows that the error using the optimized coupling conditions is two to four times smaller than for the original ones. We finally illustrated the theoretical results numerically for several test cases.

References

1. P. Angot, F. Boyer, and F. Hubert. Asymptotic and numerical modelling of flows in fractured porous media. *ESAIM: Mathematical Modelling and Numerical Analysis*, 43(2):239–275, 2009.
2. E. Flauraud, F. Nataf, I. Faille, and R. Masson. Domain decomposition for an asymptotic geological fault modeling. *Comptes Rendus Mécanique*, 331(12):849–855, dec 2003.
3. L. Formaggia, A. Fumagalli, A. Scotti, and P. Ruffo. A reduced model for darcy's problem in networks of fractures. *ESAIM: Mathematical Modelling and Numerical Analysis*, 48(4):1089–1116, 2014.
4. M. J. Gander. Optimized Schwarz methods. *SIAM J. Numer. Anal.*, 44(2):699–731, 2006.
5. M. J. Gander. Schwarz methods over the course of time. *ETNA*, 31:228–255, 2008.
6. M. J. Gander and L. Halpern. A simple finite difference discretization for ventcell transmission conditions at cross points. In *Domain Decomposition Methods in Science and Engineering XXVI*, LNCSE. Springer-Verlag.
7. M. J. Gander, J. Hennicker, and R. Masson. Asymptotic analysis for the coupling between subdomains in discrete fracture matrix models. In *Domain Decomposition Methods in Science and Engineering XXV*, LNCSE. Springer-Verlag, 2019.
8. M. J. Gander, J. Hennicker, and R. Masson. Modeling and analysis of the coupling in discrete fracture matrix models. *SIAM J. Numer. Anal.*, 59(1):195–218, 2021.
9. J. Hennicker. *Hybrid dimensional modeling of multi-phase Darcy flows in fractured porous media*. PhD thesis, Université Côte d'Azur, 2017.
10. V. Martin, J. Jaffré, and J. E. Roberts. Modeling fractures and barriers as interfaces for flow in porous media. *SIAM Journal on Scientific Computing*, 26(5):1667–1691, 2005.
11. E. Sánchez-Palencia. Problèmes de perturbations liés aux phénomènes de conduction à travers des couches minces de grande résistivité. *J. Math. Pures et Appl.*, 53(9):251–269, 1974.